Cell Metabolism
Article

The Asparaginyl Hydroxylase Factor Inhibiting HIF-1α Is an Essential Regulator of Metabolism

Na Zhang,[1] Zhenxing Fu,[2] Sarah Linke,[4] Johana Chicher,[5] Jeffrey J. Gorman,[5] DeeAnn Visk,[3] Gabriel G. Haddad,[3] Lorenz Poellinger,[6] Daniel J. Peet,[4] Frank Powell,[2] and Randall S. Johnson[1,*]
[1]Molecular Biology Section, Division of Biological Sciences, University of California, San Diego, La Jolla, CA 92093, USA
[2]Department of Medicine
[3]Department of Pediatrics
School of Medicine, University of California, San Diego, La Jolla, CA 92093, USA
[4]School of Molecular and Biomedical Science, University of Adelaide, Adelaide, SA 5005, Australia
[5]Protein Discovery Centre, Queensland Institute of Medical Research, PO Royal Brisbane Hospital, QLD 4029, Australia
[6]Karolinska Institute, Stockholm S-17177, Sweden
*Correspondence: rsjohnson@ucsd.edu
DOI 10.1016/j.cmet.2010.03.001

SUMMARY

Factor inhibiting HIF-1α (FIH) is an asparaginyl hydroxylase. Hydroxylation of HIF-α proteins by FIH blocks association of HIFs with the transcriptional coactivators CBP/p300, thus inhibiting transcriptional activation. We have created mice with a null mutation in the *FIH* gene and found that it has little or no discernable role in mice in altering classical aspects of HIF function, e.g., angiogenesis, erythropoiesis, or development. Rather, it is an essential regulator of metabolism: mice lacking FIH exhibit reduced body weight, elevated metabolic rate, hyperventilation, and improved glucose and lipid homeostasis and are resistant to high-fat-diet-induced weight gain and hepatic steatosis. Neuron-specific loss of FIH phenocopied some of the major metabolic phenotypes of the global null animals: those mice have reduced body weight, increased metabolic rate, and enhanced insulin sensitivity and are also protected against high-fat-diet-induced weight gain. These results demonstrate that FIH acts to a significant degree through the nervous system to regulate metabolism.

INTRODUCTION

Metabolic response is the act of balancing demand against substrate availability. A key element of this balance is oxygen availability, which influences both the rate and the mechanism of substrate utilization for energy production (Semenza, 2007). The hypoxia-inducible factors act as regulators of transcriptional response to low oxygen. They respond to a wide range of oxygen concentrations and coordinate response via alterations in expression of at least 300 genes (Weidemann and Johnson, 2008).

The HIF response has a series of complex controls. Central is enzymatic, oxygen-dependent modification of the HIF-1α and HIF-2α proteins (Semenza, 2004). This depends on availability of oxygen for catalysis of two different modifications of HIF-α proteins. The first oxygen-dependent covalent changes involve prolyl hydroxylases, or PHDs. These hydroxylate highly conserved prolines in HIF-α transcription factors; this regulates ubiquitination and destruction of HIF-α proteins (Semenza, 2007). The second category requires a factor termed FIH (encoded by the *Hif1an* gene); this catalyzes asparagine hydroxylation, which blocks association of HIF-α transcription factors with CBP/p300 transcriptional coactivators (Lando et al., 2002; Mahon et al., 2001). Null mutations in the *PHDs* and in the von Hippel-Lindau tumor suppressor gene (VHL) that mediates HIF-α ubiquitination all generally exhibit some of the archetypal features of increased HIF activation, e.g., increased vascularization and high levels of erythropoiesis (Aragonés et al., 2008; Bishop et al., 2008; Gnarra et al., 1997; Takeda et al., 2006, 2008).

The *FIH* gene has been associated with hydroxylation events in a range of other substrates as well, including those in the Notch pathway (Coleman et al., 2007; Zheng et al., 2008) and the tankyrase protein (Cockman et al., 2009); given this, a genetic examination of the role of the *FIH* gene is essential to begin a determination of its actual role in animal physiology. We have found that loss of FIH results in a wide-ranging derangement of physiological response and causes a hypermetabolic phenotype, but results in few of the classical effects of HIF activation in vivo. These data indicate that inhibition of this enzyme could provide a unique mechanism for manipulation of metabolism.

RESULTS

Targeting of the *FIH* Gene Creates a Null Allele

As can be seen in Figure 1A, the *FIH* gene product is expressed in a wide range of tissues. We created a conditional null mutation of the gene, as shown in Figure 1B, with a targeting efficiency of 2 clones generated for approximately 1800 ES cell clones screened (Figure S1A). Both isolated clones were able to produce germline transmission of the altered allele. Mutant animals were crossed with the EIIa-Cre transgenic line to generate complete nullizygous alleles ($FIH^{\Delta 2}$) and conditional alleles (FIH^{flox}), as shown in (d) and (e) of Figure 1B (Lakso et al., 1996).

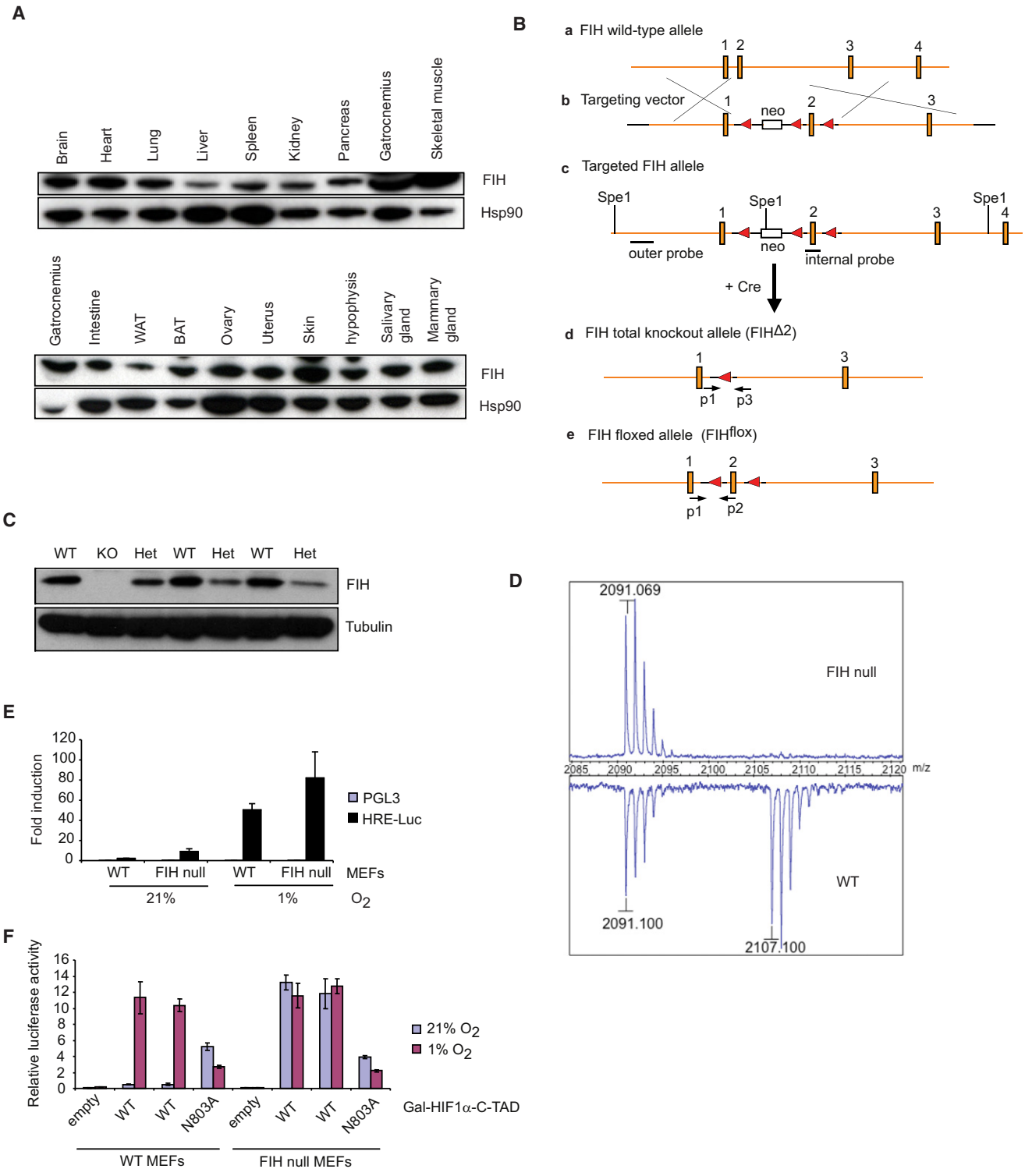

Figure 1. Generation of FIH Knockout Mice

(A) Immunoblotting for FIH in adult mouse tissues. Various organs from a 2-month-old wild-type female were harvested and frozen at −80°C before lysis. Whole-cell extracts were obtained and immunoblotted for FIH. Hsp90 was used for the loading control.

(B) Strategy of targeting the *FIH* gene. The genomic wild-type FIH locus around exons 1–4 (filled boxes) is shown (a). A neo cassette (open box) and a *loxP* site (filled triangle) from the targeting vector (b) were introduced upstream and downstream of exon 2 by homologous recombination (c), respectively. Restriction sites (SpeI) and positions of outer and internal probes for Southern blotting are indicated. After Cre-mediated excision, the FIH total knockout (KO) allele ($FIH^{\Delta 2}$) (d) and the FIH floxed allele (FIH^{flox}) (e) were obtained. PCR primers used for genotyping (p1, p2, p3) are indicated (arrows).

Crosses of FIH$^{\Delta 2}$ heterozygous animals resulted in animals homozygous for the *FIH* null allele, which were verified for loss of protein (Figure 1C). Genotypes were also confirmed by PCR analysis (Figure S1B).

The *FIH* gene encodes an asparaginyl hydroxylase that acts on the C-terminal activation domain (C-TAD) of HIF-α proteins (Lando et al., 2002). To determine whether deletion of the *FIH* gene results in elimination of hydroxylation of the C-TAD of the HIF-α proteins, a cloned and tagged C-TAD was stably transfected into MEFs generated from FIH^{df} embryos (exon2 of the *FIH* gene is flanked by two *loxP* sites). These cells were then treated with a Cre recombinase expression construct-containing adenovirus, and control and FIH null cells were created from untreated and treated cells, respectively. Mass spectrometric analysis of the C-TAD region, as seen in Figure 1D, showed that loss of FIH completely eliminated detectable hydroxylation of the asparagine residue within the C-TAD.

Transcriptional Activation of HIF Target Genes via C-TAD Is Controlled by FIH

Gene expression assays indicated that loss of FIH in MEFs caused modest increases in transcription from an HRE reporter in both normoxic and hypoxic conditions (Figure 1E). Expression driven by a Gal-HIF-1α-C-TAD construct, where expression is dependent on C-TAD activity, shows that loss of FIH eliminates differences in hypoxic versus normoxic expression (Figure 1F). This occurs through a mechanism dependent on an intact asparagine at residue 803 in the C-TAD, as mutation of this residue makes the construct insensitive to the absence of FIH (Figure 1F).

Gene Expression Analysis Demonstrates a Selective Clamp Function for FIH

Gene expression levels for a number of genes were surveyed, but effects on HIF target genes were modest in cells nullizygous for FIH (Figure 2A). The HIF target genes *vascular endothelial growth factor* (*Vegf*), *phosphoglycerate kinase* (*Pgk*), and *glucose transporter-1* (*Glut-1*) were all minimally affected (Figure 2A).

As can be seen in Figure 2B, loss of the FIH gene results in a small decrease in cell growth. To determine the effect of the two factors together on this process, we crossed animals carrying the conditional allele of the *VHL* gene (VHL^{df}) (Haase et al., 2001) and animals carrying the conditional allele of the *FIH* gene (FIH^{df}) and then derived MEFs (as described above) from resultant embryos with conditional alleles (VHL^{df}/FIH^{df}) of both the *VHL* and *FIH* genes. Figure 2C documents that overall effects on HIF-1α levels are as expected, with an increase in HIF-1α levels primarily determined by VHL.

Figures 2D and 2E show the effects on gene expression in normoxia of loss of the two factors, VHL and FIH, concurrently, and demonstrate that their deletion has at least two classes of outcome. The first, seen in the HIF target gene *Vegf*, is an approximately additive effect (Figure 2D). The second is seen in a group of genes (Table S1) that includes the *carbonic anhydrase 9* gene (*Car9*); here, loss of either VHL or FIH alone creates a small increase in gene expression, but loss of the two in tandem causes an approximate 200-fold increase in *Car9* expression (Figure 2E). Figures 2F and 2G demonstrate that in the case of both the *Vegf* and *Car9* genes, a triple deletion of VHL, FIH, and HIF-1α restores to wild-type levels increased gene expression caused by loss of VHL and FIH. A gene expression matrix analysis was carried out, and the effects are shown graphically in Figure 2H.

As shown in Figure 2I, loss of VHL has a deleterious effect on cell growth; loss of both factors has an additive negative effect. The additional loss of HIF-1α (creating VHL/FIH/HIF-1α triple null cells) restores plating efficiency to wild-type levels and indicates that overactivation of HIF-1α causes cell death in these experiments.

Loss of FIH Causes an Increase in Cellular ATP Levels and Suppresses AMPK Activation

To investigate cellular metabolism, we carried out assays on intracellular ATP levels in wild-type and mutant cells maintained at normoxia and normoglycemia. In Figure 3A, loss of FIH causes an increase in cellular ATP levels; this is suppressed in FIH/HIF-1α double null cells (Figure S2A). Total levels of AMPK protein as well as levels of activated AMPK were determined in normal as well as hypoxic and hypoglycemic cultures (Figures 3B and S2B) and showed that loss of FIH suppresses AMPK activation under hypoglycemic conditions. This suppression is diminished in FIH/HIF-1α double null cells (Figure S2B). Midgestation FIH null embryos also had suppressed AMPK activation (Figure 3C); this indicates an altered metabolic state in development.

Loss of FIH Causes a Hypermetabolic State In Vivo

Activation of HIF in animals can increase glycolysis and reduce oxygen consumption and thus elevate the respiratory exchange ratio (RER = VCO_2/VO_2), a metabolic parameter related to carbohydrate utilization (an RER that approaches 1.0 is indicative of a predominant use of carbohydrates for fuel). Although FIH mutant mice have an elevated consumption of oxygen and increased evolution of carbon dioxide under normoxic conditions (Figures 3D and 3E), RER is not changed in these mice, indicating glycolysis has not increased relative to wild-type controls (Figure 3F).

As expected from elevations in oxygen consumption, loss of FIH causes an approximate 20% increase in heat production as expressed in calories/hr/unit body mass (Figure 3G). This is accompanied by an increased mutant heart rate (Figure 3H).

Increased oxygen consumption could be caused by changes in uncoupled mitochondrial respiration. We examined the expression levels of mitochondrial uncoupling genes in brown adipose tissue (BAT), white adipose tissue (WAT), and skeletal

(C) Immunoblot analysis of E12.5 whole-embryo lysates of wild-type (WT), heterozygous (Het), and KO using FIH and tubulin antibodies.
(D) MALDI-TOF MS spectra of asparaginyl hydroxylation on HIF-1α in immortalized WT and FIH null MEFs under normoxia (21% O_2).
(E) Luciferase assay using HRE (hypoxia response element) reporter in immortalized WT and FIH null MEFs under normoxia and hypoxia (1% O_2) (n = 3/each). Luciferase activity was measured 24 hr following transfection.
(F) Luciferase assay using Gal-HIF-1α-C-TAD reporter in immortalized WT and FIH null MEFs under normoxia and hypoxia. WT is the wild-type form of HIF-1α-C-TAD. N803A is the mutant form in which asparagine 803 is mutated. Values in graphs are expressed as mean ±SEM. See also Figure S1.

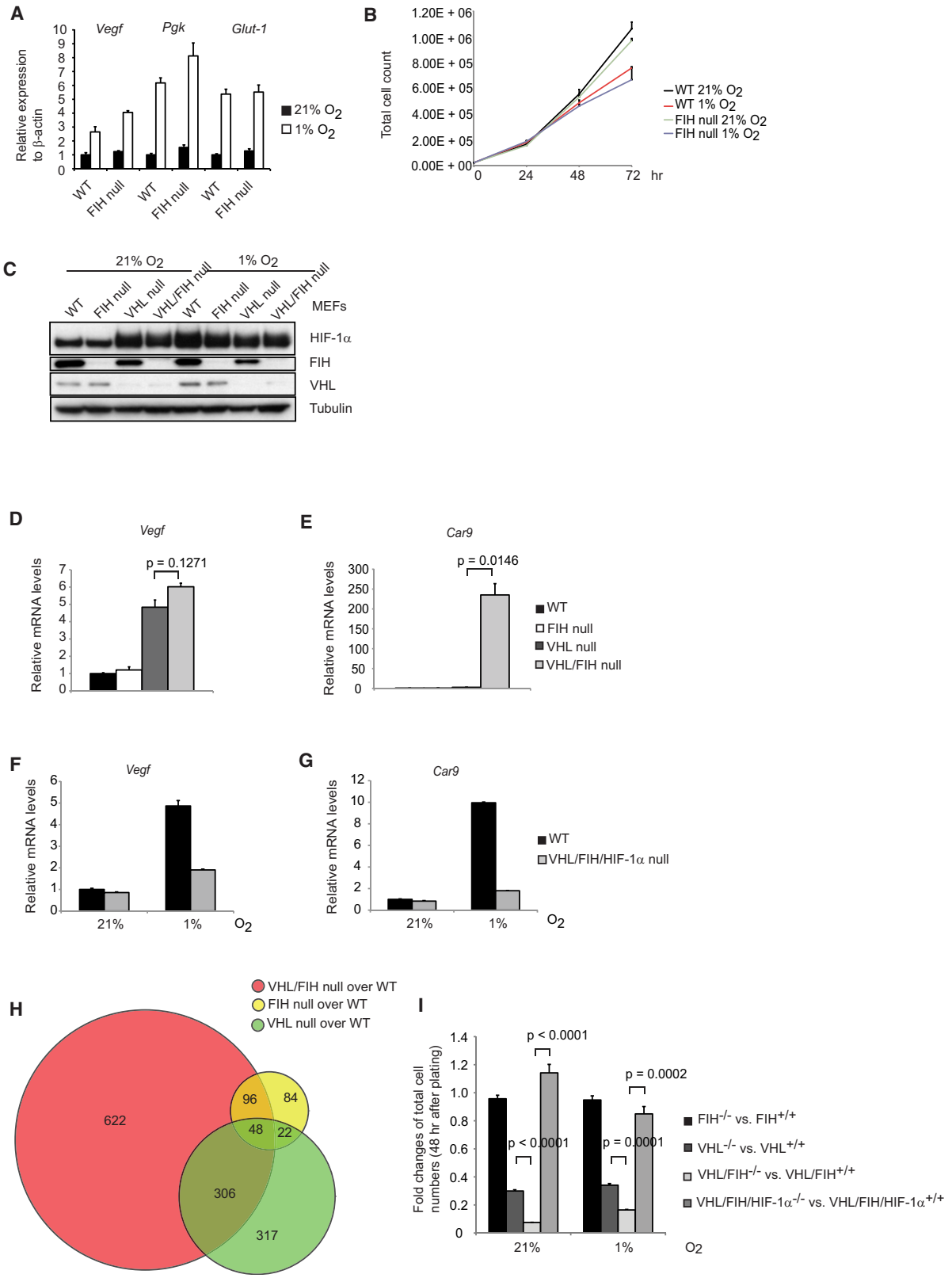
A
Vegf
Pgk
Glut-1
Relative expression to β-actin
21% O2
1% O2
WT
FIH null
B
Total cell count
WT 21% O2
WT 1% O2
FIH null 21% O2
FIH null 1% O2
hr
C
21% O2
1% O2
MEFs
HIF-1α
FIH
VHL
Tubulin
D
Vegf
p = 0.1271
Relative mRNA levels
E
Car9
p = 0.0146
WT
FIH null
VHL null
VHL/FIH null
F
Vegf
G
Car9
VHL/FIH/HIF-1α null
H
VHL/FIH null over WT
FIH null over WT
VHL null over WT
622
96
84
48
22
306
317
I
Fold changes of total cell numbers (48 hr after plating)
p < 0.0001
p = 0.0002
FIH-/- vs. FIH+/+
VHL-/- vs. VHL+/+
VHL/FIH-/- vs. VHL/FIH+/+
VHL/FIH/HIF-1α-/- vs. VHL/FIH/HIF-1α+/+

muscle (SM) and found that the *uncoupling protein 1* (*UCP1*) mRNA level in BAT from FIH nullizygous mice was significantly increased (Figure 3I). Levels of *peroxisome proliferator-activated receptor γ (PPARγ) coactivator-1α (PGC-1α)* mRNA were also increased in BAT from mutant animals (Figure 3J); PGC-1α is an important regulator of thermogenesis (Uldry et al., 2006). Expression levels of the *uncoupling protein 2* (*UCP2*) and *uncoupling protein 3* (*UCP3*) genes in BAT, WAT, and SM and the *PGC-1α* gene in WAT were similar between genotypes (Figures 3I and S3A–S3C).

Mice Lacking FIH Are Hyperventilatory and Exhibit Alkalosis

Ventilation is strongly affected by hypoxia in mammals; both tidal volume and respiratory frequency increase as oxygen levels drop (Huey et al., 2000). To investigate a potential role for FIH in hypoxic ventilation, we undertook plethysmography of the mutants (Figures 4A–4C). These analyses demonstrated that the frequency of breathing at normoxia is not elevated in FIH mutants (Figure 4A), but that the tidal volume is higher, with a mean increase of close to 30% (Figure 4B).

The tidal volume (Figure 4B) seen in wild-type mice at hypoxia is similar to that at normoxia in FIH mutants. Hyperoxia reduces mutant tidal volume: at 30% oxygen, FIH nullizygous tidal volumes are not significantly different from those of wild-type mice. This indicates that FIH may act to regulate the set point for oxygen-regulated changes in tidal volume.

The elevation in frequency of respiration relative to wild-type animals is significant only during hypoxia (Figure 4A); this indicates that a second level of compensation for hypoxia is triggered in FIH mutant animals; these mutants presumably have little capacity to increase tidal volume further and thus respond to decreased oxygenation with an increased respiratory frequency. This increase in respiratory frequency, in the presence of an increased tidal volume, could generate increased levels of blood oxygenation relative to wild-type animals. Evidence of hyperoxygenation at normoxia is seen in Table S2, where both pO_2 (partial pressure of oxygen) and SO_2 (oxygen saturation) are elevated in arterial blood gas analysis of mutants.

Analysis of minute volume (Vi, in Figure 4C), which is a measurement of total inspired air over time and thus reflects both tidal volume and frequency of respiration, shows that the greatest discrepancy between wild-type and mutant mice is at normoxia (Figure 4C). At hyperoxia, the genotypic differential in Vi is no longer statistically significant.

Increased ventilation can be due to hyperpnoea or respiratory adaptation to an increased metabolic rate; this would be accompanied by a plasma acidosis or, if compensated, a normal blood pH. If hyperventilation is occurring, however, the increased exhalation of carbon dioxide in the absence of a metabolically driven production of CO_2 causes a drop in pCO_2 (partial pressure of carbon dioxide) and an accompanying alkalosis. FIH null mutants have a clear hypocapnia (decreased pCO_2) and respiratory alkalosis (increased blood pH), characteristic of hyperventilation (Table S2).

Mice Lacking FIH Have Decreased EPO Levels in Response to Hypoxia

To further determine how hypoxic physiology is regulated by the FIH enzyme, we undertook examination of a basal response to hypoxia: increased expression of the erythropoietic hormone erythropoietin (EPO) (Semenza, 2009). Consistent with a lack of HIF-related changes in vascularization in the FIH null mutants (Figure S4C), basal levels of EPO, hematocrits, and reticulocyte counts are not different from those of wild-type animals (data not shown). This also differs from a wide range of tissue-specific deletions of both the PHDs and VHL, which exhibit increased *EPO* expression and varying degrees of polycythemia (Boutin et al., 2008; Haase et al., 2001; Peyssonnaux et al., 2007; Rankin et al., 2007; Takeda et al., 2008).

We found that global loss of FIH does alter *EPO* expression after 14 hr of exposure to hypoxia (9% O_2); levels of plasma EPO in FIH null animals are reduced by approximately 40% (Figure 4D). Renal expression of *EPO* mRNA correlates with the reduction in plasma EPO levels and is reduced by approximately 75% relative to wild-type levels posthypoxia (Figure 4E).

To determine whether this was caused by a direct effect on gene expression, we examined an *EPO*-expressing cell line, the Hep3B cell line (Figure 4F). Suppression of FIH by siRNA in these cells did not, however, alter hypoxic induction of *EPO* expression significantly (Figure 4F).

To determine whether loss of EPO inducibility in mutants occurs in other contexts, we assayed plasma EPO levels following induction of experimental anemia (Figure 4G). This assay employs phenylhydrazine (PHZ) to induce red blood cell lysis; following treatment, hematocrits in experimental animals drop, and the resulting anemia causes an increase in *EPO* expression. In these experiments, there were no significant changes in plasma EPO levels in mutants relative to wild-type animals (Figure 4G) and no alteration in induction of renal *EPO*

Figure 2. Synergistic Effects of FIH and VHL on Regulating HIF Activity In Vitro

(A) Representative quantitative PCR (qPCR) analysis of mRNA levels for *Vegf*, *Pgk*, *and Glut-1*. Immortalized WT and FIH null MEFs were treated under normoxia and hypoxia for 16 hr. Results were normalized to β-actin.

(B) Growth of WT and FIH null MEFs was examined under normoxia and hypoxia. Cells seeded at a low density were incubated in normoxic or hypoxic conditions and harvested for cell counts every 24 hr. The average cell number of triplicates for each condition is shown.

(C) Immunoblotting for HIF-1α, FIH, and VHL from whole-cell lysates of immortalized WT, FIH null, VHL null, and VHL/FIH double null MEFs. Cells were treated under normoxia or hypoxia for 16 hr before harvest. Tubulin was used as the loading control.

(D and E) Representative qPCR analysis of mRNA level for *Vegf* (D) and *Car9* (E) in WT, VHL null, and VHL/FIH null MEFs (n = 3/genotype).

(F and G) mRNA levels of both *Vegf* (F) and *Car9* (G) were restored by a triple deletion of VHL, FIH, and HIF-1α. For (D–F), cells were cultured under normoxia. Primers specific for β-actin were used for normalization.

(H) Venn diagram showing the numbers of up- and downregulated genes in MEFs using a filter of ≥2-fold change.

(I) VHL and FIH have synergistic effects on regulating cell growth. They were restored by deletion of HIF-1α. MEFs were seeded at a low density and incubated under normoxia or hypoxia for 48 hr. Cell numbers of each nullizygous MEF were counted and normalized to relative wild-type MEFs (n = 3/condition). Values in graphs are expressed as mean ±SEM; p values are from Student's t test. See also Table S1.

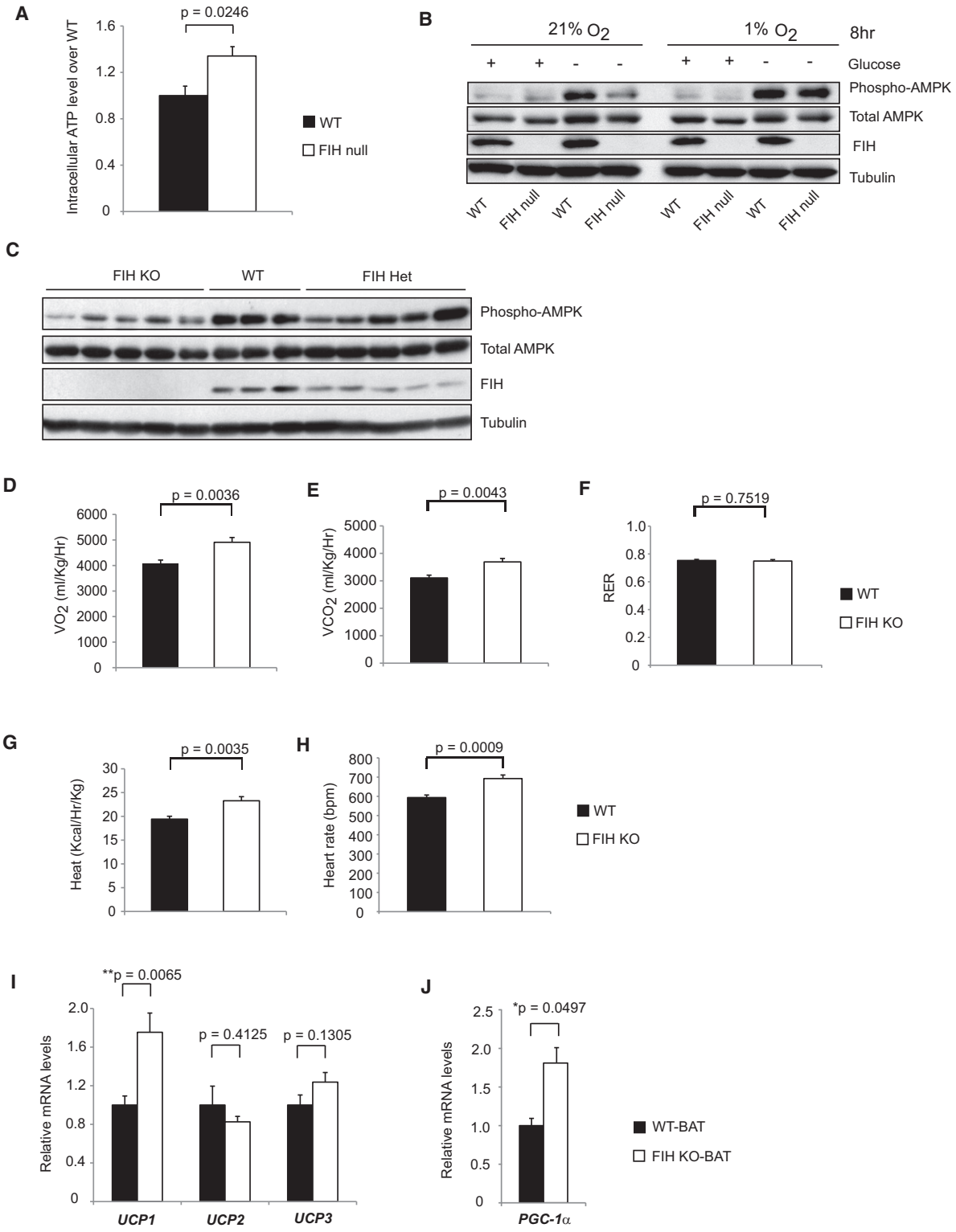

Figure 3. Hypermetabolism in FIH KO Mice

(A) Intracellular ATP levels in primary WT and FIH null MEFs under normoxia (n = 3/group).

(B) Levels of phospho-AMPK and total AMPK were measured by immunoblotting with whole-cell lysates from primary WT and FIH null MEFs treated with conditions as indicated.

(C) Immunoblotting analysis of whole-cell lysates from E12.5 WT (n = 3), FIH Het (n = 5), and FIH KO (n = 5) embryos using phospho-AMPK, total AMPK, FIH, and tubulin antibodies.

expression (Figure 4H). This demonstrates that the alteration in *EPO* expression that we see in FIH mutants is not related to direct effects on *EPO* expression in EPO-synthesizing tissues, but is correlated with altered respiration during hypoxia.

Loss of FIH Causes Decreased Body Mass and Adiposity

Loss of FIH causes an increase in both food and water consumption in conjunction with the increased metabolic rate described above (Figures 5A and 5B). Physical activity is a central aspect of energy expenditure and so was measured together with O_2 consumption. As shown in Figure 5C, a significantly higher O_2 consumption in mutants accompanied a surprising hypoactivity, especially during dark cycles.

Body weight represents to some extent a balance between energy intake and expenditure. Overall body mass in FIH nullizygous mice is lower at birth (Figure 5D) and throughout life (Figure 5E). This is accompanied by a decrease in epididymal WAT (Figure 5F and Table S4). Adipocytes from FIH nullizygous mice are significantly smaller than those from control mice (Figures 5G–5I), demonstrating decreased adiposity.

To determine the effect of FIH deletion on glucose physiology, glucose and insulin tolerance tests (GTTs and ITTs) were carried out (Figures 5J and 5K). Loss of FIH had little effect on glucose clearance, but had a significant effect on insulin sensitivity (Figure 5K). Correlated with an enhanced insulin sensitivity was a significantly lower fed plasma insulin level in mutants (Figure 5L) and improved lipid homeostasis. Serum triglyceride (TG), high-density lipoprotein (HDL) cholesterol, low-density lipoprotein (LDL) cholesterol, very-low-density lipoprotein (VLDL) cholesterol, and total serum cholesterol levels were all significantly lower in mutant animals (Table S3).

Tissue-Specific Loss of FIH Indicates that Hypermetabolism Is Neuronally Regulated under Normal Chow

We found that FIH is expressed at similar levels in different brain regions, i.e., cortex, hypothalamus, and brain stem (Figure S5A). Animals were created with a pan-neuronal loss of FIH by crossing into a background of nestin promoter-driven Cre expression. Specific deletion of FIH was confirmed by immunoblotting and quantitative PCR (Figures 6A and S5B). These tissue-specific deletion mutants are significantly smaller than controls (Figure 6B) and phenocopy the increased metabolic rate seen in global FIH null animals (Figure 6C).

To investigate whether loss of FIH in neurons affects glucose homeostasis, GTTs and ITTs were performed: neuronal FIH null mutants exhibited improved insulin sensitivity, although glucose tolerance was unchanged (Figures 6D and 6E). There was no significant difference in fasting blood glucose levels in 2-month-old animals (Figure S5C), but fasting plasma insulin levels in mutants were lower (Figure S5D), which correlates with an enhanced insulin sensitivity.

In contrast, hepatic loss of FIH in an albumin-Cre background had no effect on overall body weight and metabolic rate (Figures S6A–S6C); loss of FIH in liver did not affect glucose homeostasis (Figures S6D–S6F).

Expression of HIF-1α target genes, including *Pgk*, *Vegf*, *Glut-1*, *Bnip3*, and *Car9*, is not significantly elevated in the brains of FIH nullizygous mice (Figure S5E). This indicates that the neuronal FIH mutant phenotype is not directly related to a large and tissue-specific alteration in gene expression of HIF target genes in the central nervous system.

FIH Knockout Mice Are Protected from High-Fat-Diet-Induced Weight Gain and Hepatic Steatosis

To determine whether global deletion of FIH influences the weight gain, insulin resistance, and hepatic steatosis seen when mice are administered a high-fat diet (HFD), we fed FIH null mice and wild-type littermates for 4 months with a 60% fat diet. As can be seen in Figures 7A and S7A, this caused weight gain in both wild-type and mutant mice; however, mutants gained significantly less weight relative to wild-type animals. This divergence is not seen over time when animals are fed normal chow (Figure 7B).

We next measured individual tissue weights of liver, epididymal WAT, quadriceps, and kidney, and found that under a HFD there were significant changes in tissue/body mass ratios of liver and quadriceps in mutants relative to wild-type animals (Table S4B). FIH global deletion mice also have higher metabolic rates under HFD (Figure 7C) and no difference in GTTs (Figures 7D and S7C), but ITTs show that mutants maintain increased insulin sensitivity (Figures 7E and S7D). This is correlated with lower fasting glucose levels (Figure 7F) and fed insulin levels in mutants (Figure 7G). Although HFD increased serum cholesterol levels, FIH null mutants still showed significantly lower serum LDL/VLDL levels (Table S3).

HFD can lead to hepatic steatosis or fatty liver. Overall liver/body mass ratio was significantly decreased in FIH nullizygous mice (Figures 7I and S7B). Liver sections show that loss of FIH causes a decrease in lipid droplets (Figure 7J); quantification demonstrated that hepatic TG content of FIH nullizygous mice was reduced by 60% (Figure 7K).

Reduced lipogenesis and increased β-oxidation are possible causes of reduced steatosis: we found no changes in mRNA levels of β-oxidation enzymes, but decreases in lipogenic enzymes (e.g., Scd1). Interestingly, we also detected significantly lower hepatic PPARγ expression in FIH nullizygous livers from HFD-fed mice (Figure 7L); this is the opposite of the trend in PPARγ expression in WAT (Figure 7H) and indicates that

(D) Resting whole-body O_2 consumption (VO_2) in 2-month-old WT (n = 7) and FIH KO (n = 5) mice. Shown are the average values over 3 hr.
(E) Resting CO_2 production (VCO_2) in the same mice as in (D).
(F) RER (respiratory exchange ratio) was determined during the same period as in (D).
(G) Heat production was determined during the same measurement as in (D).
(H) Heart rates were measured in resting 2-month-old WT (n = 9) and FIH KO (n = 5) mice under normoxic condition.
(I) *UCP1*, *UCP2*, and *UCP3* mRNA levels in brown adipose tissue (BAT) from 5-month-old mice under normal chow were measured by qPCR (n = 6/genotype).
(J) *PGC-1*α mRNA levels in BAT from 5-month-old mice under normal chow were measured by qPCR (n = 6/genotype). For gene expression analysis in (I) and (J), specific primers for β-actin were used for normalization. Values shown in graphs are expressed as mean ±SEM; p values are from Student's t test. See also Figures S2 and S3.

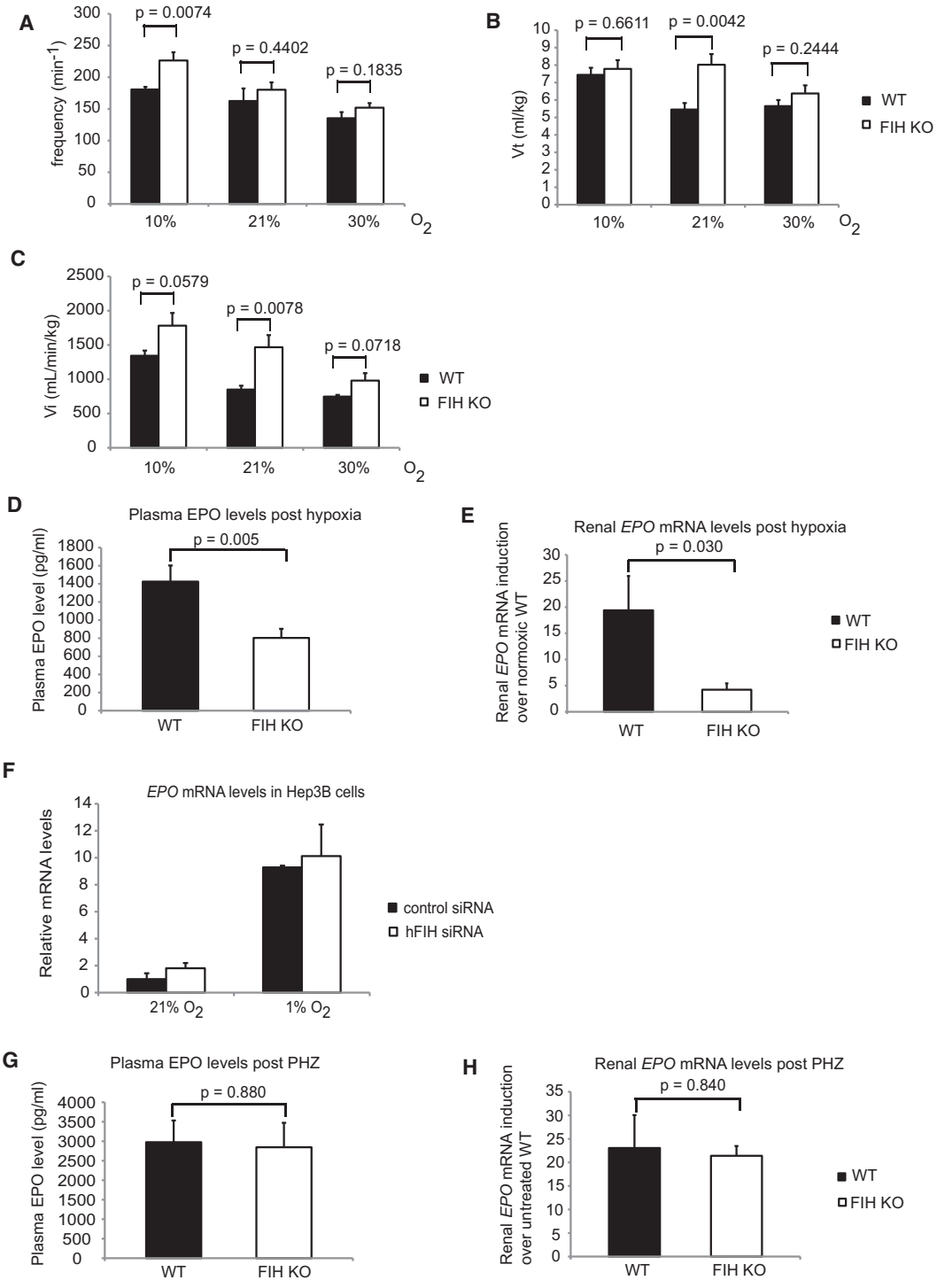

Figure 4. FIH KO Mice Are Hyperventilatory

(A) Respiration frequencies of unrestrained WT (n = 7) and FIH KO (n = 8) mice under acute hypoxia (10% O_2), room air (21% O_2), and hyperoxia (30% O_2) were measured using barometric pressure plethysmography.

(B) Tidal volume (V_t) was measured in the same assay as in (A).

(C) Inspired minute ventilation (V_i) was determined in the same assay as in (A).

(D) Plasma EPO levels in WT and FIH KO mice following acute hypoxic exposure at 9% O_2 for 14 hr (n = 15/genotype).

(E) Analysis of renal *EPO* mRNA levels in hypoxia-treated WT (n = 7) and FIH KO (n = 8) mice (9% O_2, 14 hr) by qPCR. Kidneys were collected immediately after hypoxia treatment, fast frozen in liquid N_2, and stored at −80°C before RNA isolation.

metabolic changes in PPARγ expression may help explain how FIH loss inhibits HFD-induced hepatic steatosis.

Finally, to examine whether a tissue-specific deletion of FIH in neurons also protects mutants from HFD-induced weight gain, we fed 4-week-old FIH neuronal knockout (NKO) mice and wild-type littermates HFD for 10 weeks. At 8 week and 10 week time points, FIH NKO mice fed with HFD had gained significantly less weight (Figures 7M and 7N), consistent with a role for neuronal FIH expression in regulating HFD-induced weight gain.

DISCUSSION

Together, these data indicate that FIH, the asparaginyl hydroxylase, exerts a wide-ranging control over metabolism. This is surprising from many perspectives, particularly in reference to phenotypes of other mutations in the HIF pathway. Global and conditional mutations of genes regulating HIF are generally deleterious, causing embryonic lethality or significant changes in vascularization or erythropoiesis. The data presented here demonstrate that the two hydroxylase-regulated HIF control pathways play very different roles in vivo.

The FIH enzyme has a higher affinity for oxygen than the PHD enzymes (Koivunen et al., 2004; Peet et al., 2004). Thus, FIH could suppress HIF at different oxygen concentrations from those where the PHDs are most active. We find little evidence for this in vitro, where alterations in gene expression caused by FIH are for the most part small at both normoxia and hypoxia. It is clear, however, that some genes, e.g., *Car9*, are highly dependent on FIH control when VHL is absent; it is intriguing to speculate that further investigation of genes that show a requirement for both elements of hydroxylase control may unveil a functional relationship among such targets.

We have found that cellular metabolism is altered by deletion of FIH. Curiously, this alteration in metabolism, with an increase in intracellular ATP levels in MEFs and a repression of AMP kinase activation in developing embryos, is not accompanied by the acidosis and increased glycolysis thought to typify increased HIF activation in animals. Analysis of whole-body energy expenditure demonstrated that there is an acceleration of metabolic rate in FIH mutants, but there is no evidence of increases in glycolysis. Thus, the altered metabolism of these mutants is not simply a change in HIF activation leading to increases in glycolysis and suppression of oxidative metabolism. *UCP1* and *PGC-1α* expression in BAT were significantly elevated in FIH KO mice, indicating increased energy expenditure in FIH KO mice may be due to increased thermogenesis in BAT. Deletion of PHD1 in mice results in reduced O_2 consumption by attenuating glucose oxidation; this was dependent on HIF function (Aragonés et al., 2008, 2009). As discussed above, different affinities of PHD1 and FIH for oxygen may represent a possible explanation for why they exhibit differential effects on energy expenditure, but further investigation is needed to understand this phenomenon.

Our data also connect the function of the FIH oxygen sensor with glucose and lipid metabolism in vivo. We have found that FIH null animals are smaller in size and weigh less when fed normal chow. They exhibit increased insulin sensitivity, which is correlated with significantly decreased plasma insulin levels. In contrast, there is no difference in glucose tolerance. FIH null mutants also show improved lipid homeostasis, with large reductions in serum TG and cholesterol levels. Mice with tissue-specific deletions of FIH demonstrate that deletion of FIH in neurons also leads to decreased body weight, increased energy expenditure, and improved insulin sensitivity and thus phenocopy global FIH null animals. Hepatic deletion animals did not have any of these metabolic phenotypes, arguing for a predominant role for FIH in the nervous system; clearly, further investigation of this is needed to isolate neuronal FIH-regulated pathways of metabolic control.

Deletion of FIH protects against HFD-induced weight gain and hepatic steatosis. The former may be explained by increased energy expenditure and improved insulin sensitivity in FIH global null animals. The latter is correlated with decreased expression of lipogenic genes in liver and increased adiponectin expression in WAT. Interestingly, FIH neuronal null mice are also protected against HFD-induced weight gain.

The findings described here indicate a specific role for FIH in the process of respiratory control: maintenance of a set point for normoxic respiration. In the absence of FIH, tidal volumes at normoxia are equivalent to those seen in severely hypoxic wild-type animals. This increased tidal volume is not constitutive: when breathing 30% oxygen, FIH mutant mice decrease tidal volumes to levels not significantly different from those of wild-type mice. This indicates that loss of FIH has shifted oxygen-mediated control of respiration to a lower response point.

The regulation of chronic ventilatory adaptation has been shown to be a function of the HIF pathway in mice heterozygous for HIF-1α (Kline et al., 2002; Peng et al., 2006). Increased ventilation can be related to increases in metabolic rate; these would typically involve metabolically driven acidosis. In these mice, we see instead a respiratory alkalosis, which would indicate that some degree of hyperventilation is occurring. Hyperventilation could involve defective functioning of the carotid bodies, and the suppression of the hyperventilatory phenotype by hyperoxia in these mice could indicate an altered carotid body set point in the FIH null mice. The nestin gene, whose promoter drives Cre recombinase expression in our neuronal FIH null mice, is expressed in carotid bodies (Izal-Azcárate et al., 2008). Thus, preservation of the respiratory changes in neuronal FIH deletion could indicate that carotid body FIH is a key factor in regulating respiration. Further investigation is underway to determine this in isolated carotid bodies, with an ultimate goal of defining the mechanism of signaling controlled by FIH hydroxylation.

As discussed above, our results in global FIH null and neuron-specific FIH null animals reveal the role of this gene in regulation of metabolism. A key question is whether this is related to

(F) Representative qPCR analysis of mRNA levels for *EPO* in Hep3B cells following control or *hFIH* siRNA treatment. Cells were cultured under normoxic or hypoxic conditions for 16 hr before harvest (n = 3/condition).
(G) Plasma EPO levels in WT (n = 6) and FIH KO (n = 5) mice after overnight PHZ treatment.
(H) qPCR analysis of renal *EPO* expression in PHZ-treated mice (same as those in G). Results in (E), (F), and (H) were normalized to β-actin. Values shown in graphs are expressed as mean ±SEM; p values are from Student's t test. See also Table S2.

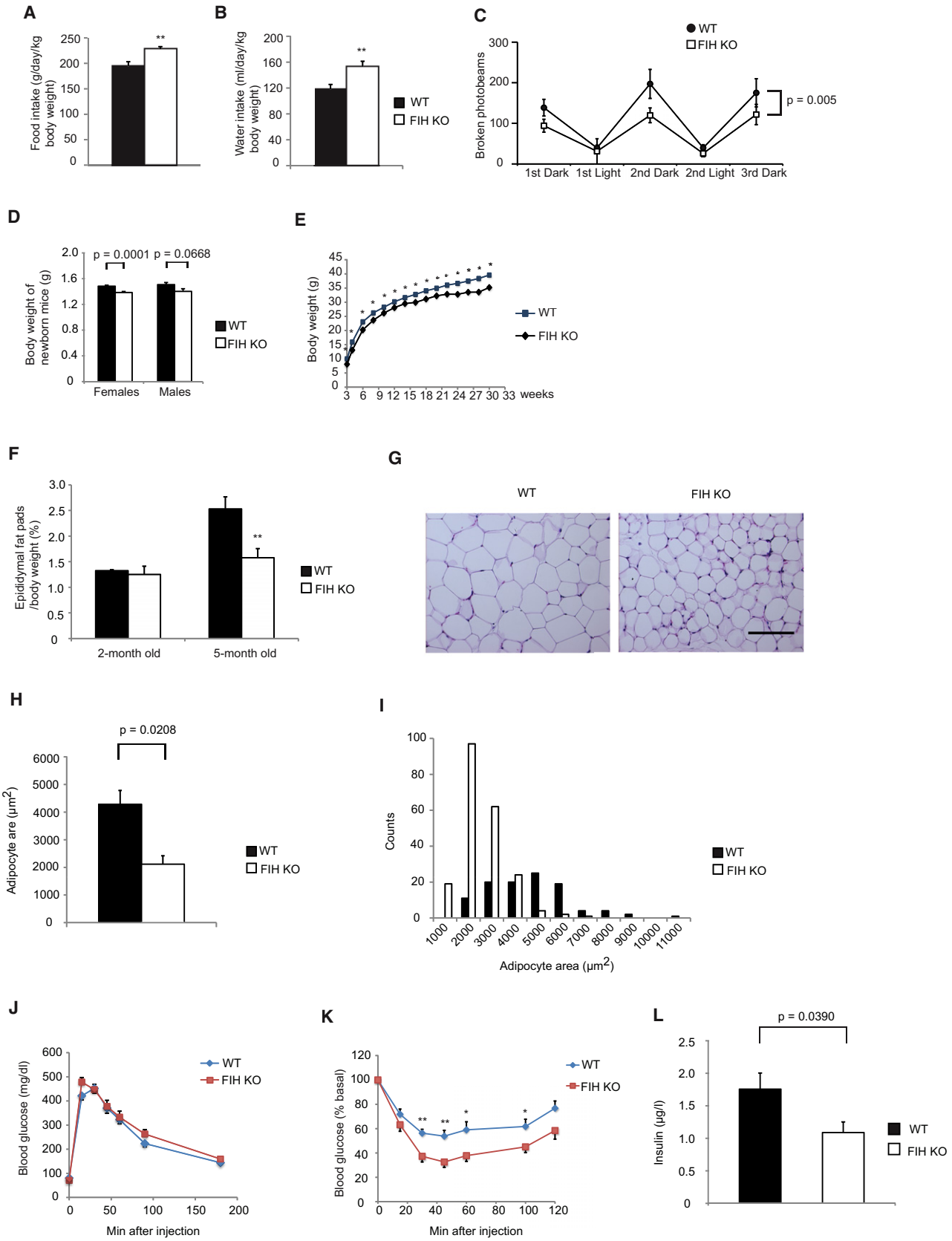
A
Food intake (g/day/kg body weight)
250
200
150
100
50
0
**
B
Water intake (ml/day/kg body weight)
200
160
120
80
40
0
**
WT
FIH KO
C
WT
FIH KO
Broken photobeams
300
200
100
0
p = 0.005
1st Dark
1st Light
2nd Dark
2nd Light
3rd Dark
D
Body weight of newborn mice (g)
2.0
1.6
1.2
0.8
0.4
0
p = 0.0001
p = 0.0668
Females
Males
WT
FIH KO
E
Body weight (g)
45
40
35
30
25
20
15
10
5
0
3 6 9 12 15 18 21 24 27 30 33 weeks
WT
FIH KO
F
Epididymal fat pads /body weight (%)
3.0
2.5
2.0
1.5
1.0
0.5
0
**
2-month old
5-month old
WT
FIH KO
G
WT
FIH KO
H
p = 0.0208
Adipocyte are (μm2)
6000
5000
4000
3000
2000
1000
0
WT
FIH KO
I
Counts
100
80
60
40
20
0
1000
2000
3000
4000
5000
6000
7000
8000
9000
10000
11000
Adipocyte area (μm2)
WT
FIH KO
J
Blood glucose (mg/dl)
600
500
400
300
200
100
0
0
50
100
150
200
Min after injection
WT
FIH KO
K
Blood glucose (% basal)
120
100
80
60
40
20
0
**
**
*
*
0
20
40
60
80
100
120
Min after injection
WT
FIH KO
L
p = 0.0390
Insulin (μg/l)
2.5
2.0
1.5
1.0
0.5
0
WT
FIH KO

regulation of HIF function, or to altered activity of other putative FIH targets. Loss of VHL in hepatocytes results in a severe HIF-dependent steatosis, and deletion of HIF-1β in liver results in increased hepatic gluconeogenesis and lipogenic gene expression but reduced hepatic lipid storage (Rankin et al., 2009; Wang et al., 2009). These data indicate that HIF activation increases steatosis in the liver. However, we see reduction in steatosis following FIH deletion, which may indicate that the metabolic changes we are observing are not directly related to increased HIF activity.

Besides HIF, FIH has been shown to hydroxylate a range of other substrates in vitro; these include proteins containing ankyrin repeat domains (ARDs), such as the intracellular domain of Notch receptors (Coleman et al., 2007; Zheng et al., 2008), p105, IkBα (Cockman et al., 2006), SOCS (suppression of cytokine signaling) box protein 4 (ASB4) (Ferguson et al., 2007), MYPT1 (Webb et al., 2009), Tankyrase-2, Rabankyrin-5, and RNase L (Cockman et al., 2009). This range of substrates has complicated the determination of direct FIH action, as the intersecting functional roles between these hydroxylation events are potentially large. As a further complication, one postulated role for the association of FIH with an ARD-containing substrate has been that they act to sequester FIH from HIF and thus potentiate HIF activation (Coleman and Ratcliffe, 2009; Wilkins et al., 2009). Our studies provide useful genetic mouse models for further investigating the physiological outcome of FIH hydroxylation on these substrates.

In conclusion, our data clearly show that the oxygen sensor FIH regulates respiration, energy balance, and lipid metabolism. They also demonstrate a role for neuronal FIH in regulation of body mass, energy expenditure, and insulin sensitivity. Thus, FIH is a ready target for broad-spectrum pharmacological inhibition of hydroxylase activation and, in particular, FIH-specific inhibitors (Banerji et al., 2005; Nagel et al., 2010). Our data indicate that such inhibitors, especially those able to inhibit FIH function in neurons, might have significant therapeutic potential in reducing body weight and increasing insulin sensitivity.

EXPERIMENTAL PROCEDURES

Generation of FIH KO Mice

The targeting vector was constructed by inserting three fragments of the *FIH* gene from murine Sv129 embryonic stem (ES) cells into pFlox$^{\Delta TK}$ (gift of S. Hedrick). Offspring containing the modified FIH allele were mated with EIIa-Cre transgenic mice (gift of C. Murre) to generate FIH$^{\Delta 2/+}$ and FIH$^{flox/+}$ mice. FIH$^{\Delta 2/+}$ mice were bred to obtain FIH KO mice (FIH$^{\Delta 2/\Delta 2}$). FIH$^{flox/+}$ mice were bred to obtain FIH^{df} mice.

Animal Experiments

All animal experiments were performed according to the animal protocol approved by the Institutional Animal Care and Use Committee. Albumin-Cre and Nestin-Cre mice were obtained from Jackson Laboratory.

Immunoblotting

Immunoblotting analysis was performed using antibodies as described in the Supplemental Experimental Procedures.

Quantitative PCR Analysis of Gene Expression and Gene Deletion

Sequences for the primers and probes of mouse genes used in this study are found in the Supplemental Experimental Procedures.

Cell Culture

Cells were cultured in DMEM. Mouse embryonic fibroblasts (MEFs) were isolated from E12.5 embryos and immortalized by stable transfection with SV40 large T antigen. FIH^{df}, VHL^{df}, VHL^{df}/FIH^{df}, VHL^{df}/FIH^{df}/HIF-1α^{df}, and FIH^{df}/HIF-1α^{df} MEFs were transiently infected with adenovirus expressing β-galactosidase or Cre recombinase to obtain WT and null MEFs.

Measurement of Free ATP in MEFs

Free ATP in primary MEFs was measured using ATP Bioluminescence Assay Kit CLS II (#11699695001, Roche Diagnostics GmbH; Mannheim, Germany) in accordance with the protocol provided by the manufacturer.

Transfection and Luciferase Assay

WT and FIH null MEFs were transfected by Lipofectamine 2000 (Invitrogen; Carlsbad, CA) with pGL3 and pGL3-HRE plasmids. pRSV-β-gal was also cotransfected into cells for normalization. One day after transfection, cells were incubated in normoxic or hypoxic conditions for 18 hr.

Mass Spectrometry

Mass spectrometry methods are described in detail in the Supplemental Experimental Procedures.

Microarray Analysis

Total RNA for microarray analysis was extracted from WT, FIH null, VHL null, and VHL/FIH null MEFs under normoxic conditions; arrays were GeneChip Mouse Genome 430 2.0 Array (Affymetrix, Inc.; Santa Clara, CA). Duplicates were performed for each sample. Venn diagram was generated by using GeneSpring GX 9.0 software.

Metabolic Cage Studies

Energy expenditure of FIH KO mice and their WT littermates was measured by using the Columbus Instruments Oxymax System.

Food and water intake and physical activity of mice were measured using the comprehensive lab animal monitoring system (CLAMS, Columbus Instruments; Columbus, OH).

Figure 5. Global Loss of FIH Causes Decreased Body Mass, Decreased Adiposity, and Increased Insulin Sensitivity

(A) Food intake was measured in WT and KO mice (n = 8/genotype) over 3 day/night cycles as monitored by CLAMS.
(B) Water intake was measured in the same assay as in (A).
(C) Physical activity was measured in the same assay as in (A) and (B). p = 0.005 by two-way ANOVA.
(D) Body weights of newborn WT and KO mice. n = 17–18 for females and n = 11–14 for males, respectively.
(E) FIH KO mice are significantly smaller than their WT littermates. Growth curves show the average weights of WT (n = 34) and KO (n = 22) males. *p < 0.05.
(F) Epididymal white fat pad weight normalized with body weight was measured from 2-month-old and 5-month-old WT and KO male mice. **p < 0.01.
(G) Representative images of H&E-stained epididymal WAT sections from 5-month-old WT and KO mice fed with normal chow (NC). The scale bar represents 100 μm.
(H) Epididymal adipocyte areas were measured from 5-month-old WT and KO mice. n = 3/genotype.
(I) Counts of adipocytes in different sizes from the same mice used in (H).
(J) Glucose tolerance test (GTT) was measured for 18 hr fasting 2-month-old WT and KO mice fed with NC (2 g D-glucose/kg body weight). n = 10/genotype.
(K) Insulin tolerance test (ITT) was performed on 4 hr fasting 2-month-old WT and KO mice fed with NC (0.75 U/kg body weight). n = 10–11/genotype. *p < 0.05, **p < 0.01.
(L) Fed insulin levels were measured on 5-month-old WT and KO mice. n = 9/genotype. Values shown in graphs are expressed as mean ±SEM; p values are from Student's t test (except C). See also Figure S4 and Tables S3 and S4.

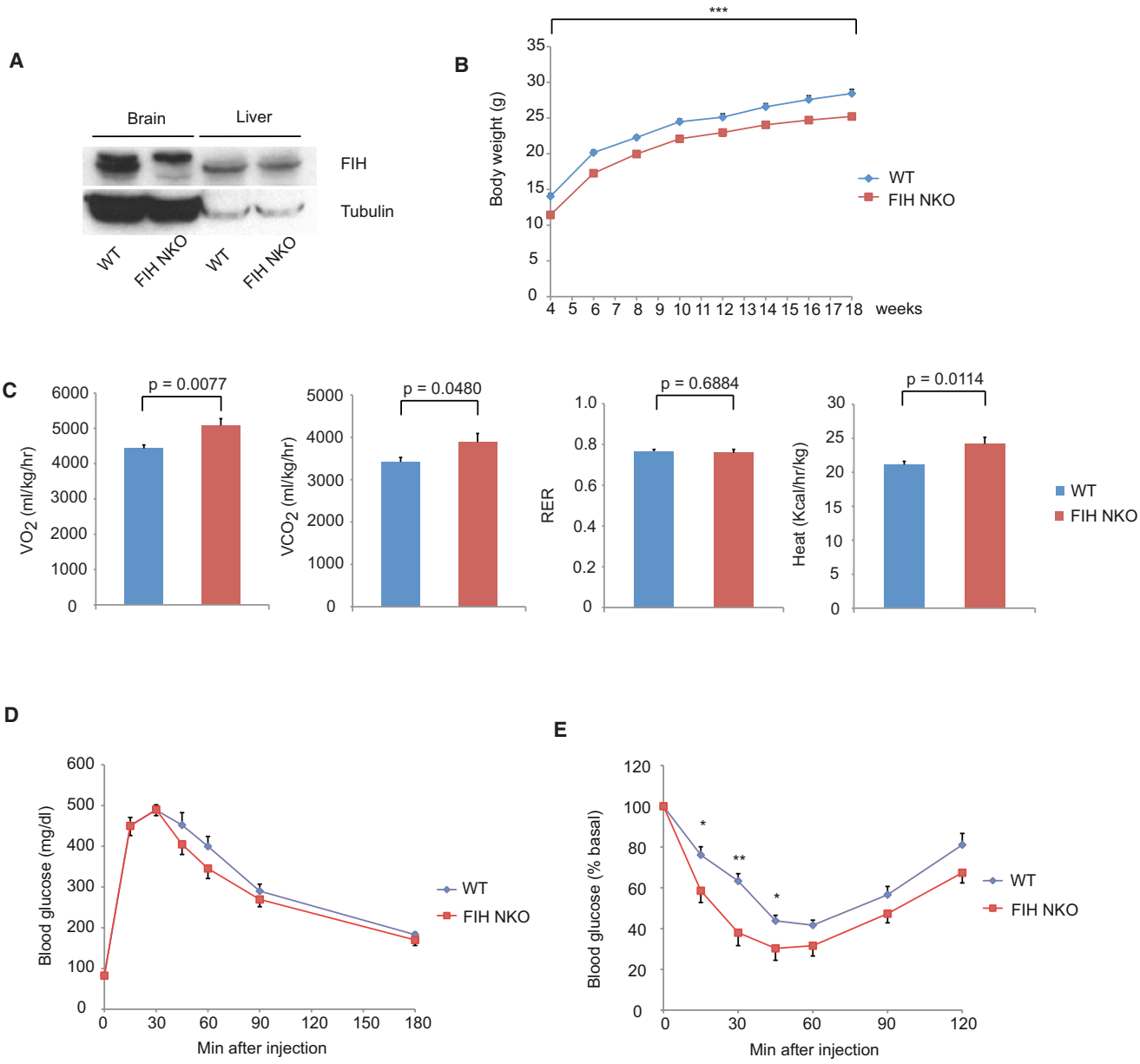

Figure 6. Neuron-Specific Loss of FIH Indicates that Hypermetabolism Is Neuronally Regulated under Normal Chow

(A) Immunoblot analysis of whole-cell lysates of brain and liver samples from FIH neuron-specific knockout mice (FIH NKO) and WT mice using FIH and tubulin antibodies. The upper bands in brain samples are nonspecific.

(B) Growth curves of FIH NKO (n = 17) and their WT (n = 15) littermates under normal chow. ***$p < 0.001$.

(C) Resting whole-body VO_2, VCO_2, RER, and heat production in 2-month-old WT (n = 7) and FIH NKO (n = 5) mice. Shown are the average values over 3 hr.

(D) GTTs were measured for 18 hr fasting 2-month-old WT (n = 6) and FIH NKO (n = 6) mice (2 g D-glucose/kg body weight).

(E) ITTs were performed on 4 hr fasting 2-month-old WT (n = 7) and FIH NKO (n = 6) mice (0.75 U/kg body weight). *$p < 0.05$, **$p < 0.01$. Values shown in graphs are expressed as mean ±SEM; p values are from Student's t test. See also Figures S5 and S6.

Hypoxia Exposure

For acute hypoxia exposure, age-matched FIH KO mice and their wild-type littermates were exposed to 9% O_2 for 14 hr in hypoxia chamber (Biospherix; Lacona, NY).

PHZ-Induced Anemia

PHZ (60 mg/kg body weight, Sigma-Aldrich; St. Louis) dissolved in sterile phosphate-buffered saline was injected intraperitoneally into 2-month-old mice to induce hemolysis. Eighteen hours after administration, tissue and plasma samples were collected for analysis.

EPO ELISA

Plasma EPO levels were determined by using the Mouse EPO ELISA kit (R&D Systems; Minneapolis, MN).

Ventilation Measurement

Ventilation was measured in unrestrained 2-month-old mice using barometric pressure plethysmography as described previously for rats (Reid and Powell, 2005), with modifications to the chamber volumes and flows appropriate for mice and a new analog-digital recording system and custom Matlab analysis routine.

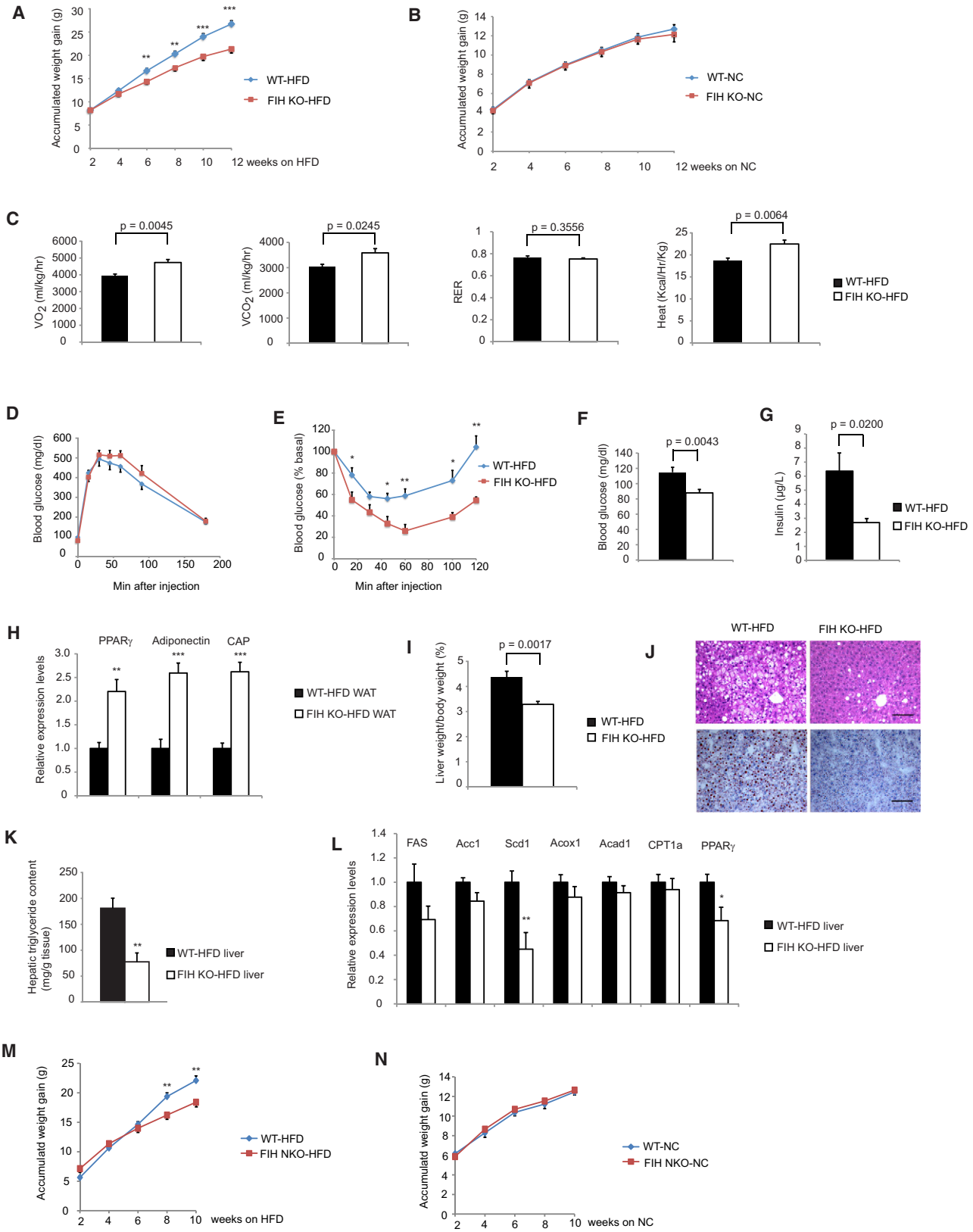
A
Accumulated weight gain (g)
WT-HFD
FIH KO-HFD
12 weeks on HFD
B
Accumulated weight gain (g)
WT-NC
FIH KO-NC
12 weeks on NC
C
p = 0.0045
VO2 (ml/kg/hr)
p = 0.0245
VCO2 (ml/kg/hr)
p = 0.3556
RER
p = 0.0064
Heat (Kcal/Hr/Kg)
WT-HFD
FIH KO-HFD
D
Blood glucose (mg/dl)
Min after injection
E
Blood glucose (% basal)
WT-HFD
FIH KO-HFD
Min after injection
F
p = 0.0043
Blood glucose (mg/dl)
G
p = 0.0200
Insulin (μg/L)
WT-HFD
FIH KO-HFD
H
PPARγ
Adiponectin
CAP
Relative expression levels
WT-HFD WAT
FIH KO-HFD WAT
I
p = 0.0017
Liver weight/body weight (%)
WT-HFD
FIH KO-HFD
J
WT-HFD
FIH KO-HFD
K
Hepatic triglyceride content (mg/g tissue)
WT-HFD liver
FIH KO-HFD liver
L
FAS
Acc1
Scd1
Acox1
Acad1
CPT1a
PPARγ
Relative expression levels
WT-HFD liver
FIH KO-HFD liver
M
Accumulatd weight gain (g)
WT-HFD
FIH NKO-HFD
weeks on HFD
N
Accumulatd weight gain (g)
WT-NC
FIH NKO-NC
weeks on NC

Measurement of Mouse Heart Rate

According to manufacturer's protocol, the measurement was done using MouseOx Pulse Oximeter with CollarClip Sensor (STARR Life Sciences Corp.; Oakmont, PA).

High-Fat Feeding

In high-fat feeding experiments, 1-month-old males were fed with HFD (60% fat content, Research Diets, Inc.; New Brunswick, NJ). Body weights were measured weekly.

Metabolic Measurements

Measurement methods for blood metabolic markers are described in the Supplemental Experimental Procedures.

Histology

Paraffin-embedded tissue sections were stained with hematoxylin and eosin (H&E) using a standard protocol. For oil red O staining, it was performed on frozen liver sections by UCSD histology core according to the standard procedure.

Quantification of adipocyte area was done on H&E-stained sections using ImageTool software.

Statistics

Values in the figures are expressed as mean ±SEM. Student's t test (unpaired, two-tailed) and two-way ANOVA were used for statistical analysis.

ACCESSION NUMBERS

Microarray data are deposited at NCBI GEO (accession number GSE20335).

SUPPLEMENTAL INFORMATION

Supplemental Information includes Supplemental Experimental Procedures, Supplemental References, seven figures, and four tables and can be found with this article online at doi:10.1016/j.cmet.2010.03.001.

ACKNOWLEDGMENTS

We thank E. Kothari and Y.H. Zhu from UCSD transgenic core for assistance with gene targeting and chimera production. We thank K. Beck for helpful discussion on generation of KO mice. We acknowledge L. Gapuz from UCSD histology core for histology.

Received: October 27, 2009
Revised: January 15, 2010
Accepted: March 1, 2010
Published online: April 15, 2010

REFERENCES

Aragonés, J., Schneider, M., Van Geyte, K., Fraisl, P., Dresselaers, T., Mazzone, M., Dirkx, R., Zacchigna, S., Lemieux, H., Jeoung, N.H., et al. (2008). Deficiency or inhibition of oxygen sensor Phd1 induces hypoxia tolerance by reprogramming basal metabolism. Nat. Genet. *40*, 170–180.

Aragonés, J., Fraisl, P., Baes, M., and Carmeliet, P. (2009). Oxygen sensors at the crossroad of metabolism. Cell Metab. *9*, 11–22.

Banerji, B., Conejo-Garcia, A., McNeill, L.A., McDonough, M.A., Buck, M.R., Hewitson, K.S., Oldham, N.J., and Schofield, C.J. (2005). The inhibition of factor inhibiting hypoxia-inducible factor (FIH) by beta-oxocarboxylic acids. Chem. Commun. (Camb.) *0*, 5438–5440.

Bishop, T., Gallagher, D., Pascual, A., Lygate, C.A., de Bono, J.P., Nicholls, L.G., Ortega-Saenz, P., Oster, H., Wijeyekoon, B., Sutherland, A.I., et al. (2008). Abnormal sympathoadrenal development and systemic hypotension in PHD3-/- mice. Mol. Cell. Biol. *28*, 3386–3400.

Boutin, A.T., Weidemann, A., Fu, Z., Mesropian, L., Gradin, K., Jamora, C., Wiesener, M., Eckardt, K.U., Koch, C.J., Ellies, L.G., et al. (2008). Epidermal sensing of oxygen is essential for systemic hypoxic response. Cell *133*, 223–234.

Cockman, M.E., Lancaster, D.E., Stolze, I.P., Hewitson, K.S., McDonough, M.A., Coleman, M.L., Coles, C.H., Yu, X., Hay, R.T., Ley, S.C., et al. (2006). Posttranslational hydroxylation of ankyrin repeats in IkappaB proteins by the hypoxia-inducible factor (HIF) asparaginyl hydroxylase, factor inhibiting HIF (FIH). Proc. Natl. Acad. Sci. USA *103*, 14767–14772.

Cockman, M.E., Webb, J.D., Kramer, H.B., Kessler, B.M., and Ratcliffe, P.J. (2009). Proteomics-based identification of novel factor inhibiting hypoxia-inducible factor (FIH) substrates indicates widespread asparaginyl hydroxylation of ankyrin repeat domain-containing proteins. Mol. Cell. Proteomics *8*, 535–546.

Coleman, M.L., and Ratcliffe, P.J. (2009). Signalling cross talk of the HIF system: involvement of the FIH protein. Curr. Pharm. Des. *15*, 3904–3907.

Coleman, M.L., McDonough, M.A., Hewitson, K.S., Coles, C., Mecinovic, J., Edelmann, M., Cook, K.M., Cockman, M.E., Lancaster, D.E., Kessler, B.M., et al. (2007). Asparaginyl hydroxylation of the Notch ankyrin repeat domain by factor inhibiting hypoxia-inducible factor. J. Biol. Chem. *282*, 24027–24038.

Ferguson, J.E., 3rd, Wu, Y., Smith, K., Charles, P., Powers, K., Wang, H., and Patterson, C. (2007). ASB4 is a hydroxylation substrate of FIH and promotes vascular differentiation via an oxygen-dependent mechanism. Mol. Cell. Biol. *27*, 6407–6419.

Gnarra, J.R., Ward, J.M., Porter, F.D., Wagner, J.R., Devor, D.E., Grinberg, A., Emmert-Buck, M.R., Westphal, H., Klausner, R.D., and Linehan, W.M. (1997). Defective placental vasculogenesis causes embryonic lethality in VHL-deficient mice. Proc. Natl. Acad. Sci. USA *94*, 9102–9107.

Figure 7. FIH KO Mice Are Protected from High-Fat-Diet-Induced Weight Gain and Hepatic Steatosis

(A) Accumulated weight gain of WT and KO mice fed with high-fat diet (HFD) for 12 weeks. n = 23 for WT mice, n = 12 for FIH KO mice, $^{**}p < 0.01$, $^{***}p < 0.001$.
(B) Accumulated weight gain of WT and KO mice fed with NC for 12 weeks. n = 16 for WT mice, n = 12 for FIH KO mice.
(C) Resting whole-body VO_2, VCO_2, RER, and heat production in WT (n = 6) and KO (n = 8) fed with HFD for 12 weeks. Shown are the average values over 3 hr.
(D) GTTs were measured for 18 hr fasting WT (n = 9) and KO (n = 7) mice fed with HFD for 12 weeks (2 g D-glucose/kg body weight).
(E) ITTs were performed on 4 hr fasting WT (n = 7) and KO (n = 5) mice fed with HFD for 12 weeks (1.0 U/kg body weight). $^{*}p < 0.05$, $^{**}p < 0.01$.
(F) Fasting blood glucose levels were measured on 18 hr fasting WT (n = 20) and KO (n = 16) mice fed with HFD for 12 weeks.
(G) Fed insulin levels were measured on WT and KO mice fed with HFD for 16 weeks. n = 6/genotype.
(H) Expression levels of genes encoding PPARγ, Adiponectin, and CAP were increased in epididymal WAT of KO mice fed with HFD. n = 6/genotype, $^{**}p < 0.01$, $^{***}p < 0.001$.
(I) Liver weight normalized with body weight from WT and KO mice fed with HFD. n = 11–19/genotype.
(J) Top: representative images of H&E-stained liver sections from WT and KO mice fed with HFD. Bottom: representative images of oil red O-stained liver sections. The scale bar represents 100 μm.
(K) Hepatic triglyceride contents were measured in WT and FIH KO livers under HFD. n = 6/genotype, $^{**}p < 0.01$.
(L) Expression levels of genes encoding lipogenic enzymes (FAS, Acc1, and Scd1), those involved in β-oxidation (Acox1, Acad1, and CPT1a), and PPARγ in livers of WT and KO mice fed with HFD. n = 6/genotype, $^{*}p < 0.05$, $^{**}p < 0.01$. WAT and liver samples used in (H)–(L) were from mice fed with HFD for 16 weeks.
(M) Accumulated weight gain of FIH neuronal KO (NKO) mice (n = 6) and their WT littermates (n = 11) fed with HFD for 10 weeks. $^{**}p < 0.01$.
(N) Accumulated weight gain of FIH NKO (n = 17) and their WT littermates (n = 13) fed with NC for 10 weeks. Values shown in graphs are expressed as mean ±SEM; p values are from Student's t test. See also Figure S7 and Tables S3 and S4B.

Haase, V.H., Glickman, J.N., Socolovsky, M., and Jaenisch, R. (2001). Vascular tumors in livers with targeted inactivation of the von Hippel-Lindau tumor suppressor. Proc. Natl. Acad. Sci. USA *98*, 1583–1588.

Huey, K.A., Low, M.J., Kelly, M.A., Juarez, R., Szewczak, J.M., and Powell, F.L. (2000). Ventilatory responses to acute and chronic hypoxia in mice: effects of dopamine D(2) receptors. J. Appl. Physiol. *89*, 1142–1150.

Izal-Azcárate, A., Belzunegui, S., San Sebastián, W., Garrido-Gil, P., Vázquez-Claverie, M., López, B., Marcilla, I., and Luquin, M.A. (2008). Immunohistochemical characterization of the rat carotid body. Respir. Physiol. Neurobiol. *161*, 95–99.

Kline, D.D., Peng, Y.J., Manalo, D.J., Semenza, G.L., and Prabhakar, N.R. (2002). Defective carotid body function and impaired ventilatory responses to chronic hypoxia in mice partially deficient for hypoxia-inducible factor 1 alpha. Proc. Natl. Acad. Sci. USA *99*, 821–826.

Koivunen, P., Hirsilä, M., Günzler, V., Kivirikko, K.I., and Myllyharju, J. (2004). Catalytic properties of the asparaginyl hydroxylase (FIH) in the oxygen sensing pathway are distinct from those of its prolyl 4-hydroxylases. J. Biol. Chem. *279*, 9899–9904.

Lakso, M., Pichel, J.G., Gorman, J.R., Sauer, B., Okamoto, Y., Lee, E., Alt, F.W., and Westphal, H. (1996). Efficient in vivo manipulation of mouse genomic sequences at the zygote stage. Proc. Natl. Acad. Sci. USA *93*, 5860–5865.

Lando, D., Peet, D.J., Gorman, J.J., Whelan, D.A., Whitelaw, M.L., and Bruick, R.K. (2002). FIH-1 is an asparaginyl hydroxylase enzyme that regulates the transcriptional activity of hypoxia-inducible factor. Genes Dev. *16*, 1466–1471.

Mahon, P.C., Hirota, K., and Semenza, G.L. (2001). FIH-1: a novel protein that interacts with HIF-1alpha and VHL to mediate repression of HIF-1 transcriptional activity. Genes Dev. *15*, 2675–2686.

Nagel, S., Talbot, N.P., Mecinović, J., Smith, T.G., Buchan, A.M., and Schofield, C.J. (2010). Therapeutic manipulation of the HIF hydroxylases. Antioxid. Redox Signal. *12*, 481–501.

Peet, D.J., Lando, D., Whelan, D.A., Whitelaw, M.L., and Gorman, J.J. (2004). Oxygen-dependent asparagine hydroxylation. Methods Enzymol. *381*, 467–487.

Peng, Y.J., Yuan, G., Ramakrishnan, D., Sharma, S.D., Bosch-Marce, M., Kumar, G.K., Semenza, G.L., and Prabhakar, N.R. (2006). Heterozygous HIF-1alpha deficiency impairs carotid body-mediated systemic responses and reactive oxygen species generation in mice exposed to intermittent hypoxia. J. Physiol. *577*, 705–716.

Peyssonnaux, C., Zinkernagel, A.S., Schuepbach, R.A., Rankin, E., Vaulont, S., Haase, V.H., Nizet, V., and Johnson, R.S. (2007). Regulation of iron homeostasis by the hypoxia-inducible transcription factors (HIFs). J. Clin. Invest. *117*, 1926–1932.

Rankin, E.B., Biju, M.P., Liu, Q., Unger, T.L., Rha, J., Johnson, R.S., Simon, M.C., Keith, B., and Haase, V.H. (2007). Hypoxia-inducible factor-2 (HIF-2) regulates hepatic erythropoietin in vivo. J. Clin. Invest. *117*, 1068–1077.

Rankin, E.B., Rha, J., Selak, M.A., Unger, T.L., Keith, B., Liu, Q., and Haase, V.H. (2009). Hypoxia-inducible factor 2 regulates hepatic lipid metabolism. Mol. Cell. Biol. *29*, 4527–4538.

Reid, S.G., and Powell, F.L. (2005). Effects of chronic hypoxia on MK-801-induced changes in the acute hypoxic ventilatory response. J. Appl. Physiol. *99*, 2108–2114.

Semenza, G.L. (2004). Hydroxylation of HIF-1: oxygen sensing at the molecular level. Physiology (Bethesda) *19*, 176–182.

Semenza, G.L. (2007). Hypoxia-inducible factor 1 (HIF-1) pathway. Sci. STKE *2007*, cm8.

Semenza, G.L. (2009). Regulation of oxygen homeostasis by hypoxia-inducible factor 1. Physiology (Bethesda) *24*, 97–106.

Takeda, K., Ho, V.C., Takeda, H., Duan, L.J., Nagy, A., and Fong, G.H. (2006). Placental but not heart defects are associated with elevated hypoxia-inducible factor alpha levels in mice lacking prolyl hydroxylase domain protein 2. Mol. Cell. Biol. *26*, 8336–8346.

Takeda, K., Aguila, H.L., Parikh, N.S., Li, X., Lamothe, K., Duan, L.J., Takeda, H., Lee, F.S., and Fong, G.H. (2008). Regulation of adult erythropoiesis by prolyl hydroxylase domain proteins. Blood *111*, 3229–3235.

Uldry, M., Yang, W., St-Pierre, J., Lin, J., Seale, P., and Spiegelman, B.M. (2006). Complementary action of the PGC-1 coactivators in mitochondrial biogenesis and brown fat differentiation. Cell Metab. *3*, 333–341.

Wang, X.L., Suzuki, R., Lee, K., Tran, T., Gunton, J.E., Saha, A.K., Patti, M.E., Goldfine, A., Ruderman, N.B., Gonzalez, F.J., and Kahn, C.R. (2009). Ablation of ARNT/HIF1beta in liver alters gluconeogenesis, lipogenic gene expression, and serum ketones. Cell Metab. *9*, 428–439.

Webb, J.D., Murányi, A., Pugh, C.W., Ratcliffe, P.J., and Coleman, M.L. (2009). MYPT1, the targeting subunit of smooth-muscle myosin phosphatase, is a substrate for the asparaginyl hydroxylase factor inhibiting hypoxia-inducible factor (FIH). Biochem. J. *420*, 327–333.

Weidemann, A., and Johnson, R.S. (2008). Biology of HIF-1alpha. Cell Death Differ. *15*, 621–627.

Wilkins, S.E., Hyvärinen, J., Chicher, J., Gorman, J.J., Peet, D.J., Bilton, R.L., and Koivunen, P. (2009). Differences in hydroxylation and binding of Notch and HIF-1alpha demonstrate substrate selectivity for factor inhibiting HIF-1 (FIH-1). Int. J. Biochem. Cell Biol. *41*, 1563–1571.

Zheng, X., Linke, S., Dias, J.M., Zheng, X., Gradin, K., Wallis, T.P., Hamilton, B.R., Gustafsson, M., Ruas, J.L., Wilkins, S., et al. (2008). Interaction with factor inhibiting HIF-1 defines an additional mode of cross-coupling between the Notch and hypoxia signaling pathways. Proc. Natl. Acad. Sci. USA *105*, 3368–3373.